Available online at www.sciencedirect.com
ScienceDirect
Biochemical and Biophysical Research Communications 363 (2007) 1050–1056
BBRC
www.elsevier.com/locate/ybbrc

Crystal structure of homoserine *O*-acetyltransferase from *Leptospira interrogans*

Mingzhu Wang [a,b,c,1], Lin Liu [a,b,1], Yanli Wang [a,b], Zhiyi Wei [a,b], Ping Zhang [a,b], Yikun Li [a,b], Xiaohua Jiang [a,b], Hang Xu [a,*], Weimin Gong [a,b,*]

[a] *National Laboratory of Biomacromolecules, Institute of Biophysics, Chinese Academy of Sciences, 15 Datun Road, Chaoyang District, Beijing 100101, PR China*
[b] *School of Life Sciences, IBP-USTC Joint Laboratory for Protein Sciences, University of Science and Technology of China, Hefei, Anhui 230026, PR China*
[c] *Graduate University of Chinese Academy of Sciences, 19 Yuquan Road, Shijingshan District, Beijing 100049, PR China*

Received 22 August 2007
Available online 4 September 2007

Abstract

Homoserine *O*-acetyltransferase (HTA, EC 2.3.1.31) initiates methionine biosynthesis pathway by catalyzing the transfer of acetyl group from acetyl-CoA to homoserine. This study reports the crystal structure of HTA from *Leptospira interrogans* determined at 2.2 Å resolution using selenomethionyl single-wavelength anomalous diffraction method. HTA is modular and consists of two structurally distinct domains—a core α/β domain containing the catalytic site and a helical bundle called the lid domain. Overall, the structure fold belongs to α/β hydrolase superfamily with the characteristic 'catalytic triad' residues in the active site. Detailed structure analysis showed that the catalytic histidine and serine are both present in two conformations, which may be involved in the catalytic mechanism for acetyl transfer.

Keywords: Homoserine *O*-acetyltransferase; Crystal structure; α/β hydrolase superfamily; Catalytic triad; Double conformations

Although diet is the sole source of methionine for mammals, plants and most micro-organisms can synthesize this essential amino acid. Methionine is synthesized de novo by plants and microbes through three major precursors, *O*-acetyl-, *O*-succinyl-, and *O*-phosphoryl-homoserine [1–4]. Gram-positive bacteria, yeast and fungi, initiate methionine biosynthesis by acetylating homoserine to yield *O*-acetylhomoserine (OAH), in which the acetyl group is donated by acetyl-CoA. OAH can then be converted to methionine via either transsulfuration or direct sulfhydrylation pathways. For both pathways the formation of the common precursor OAH is catalyzed by homoserine *O*-acetyltransferase (HTA, EC 2.3.1.31) [5,6]. Since methionine biosynthesis machinery is absent in mammals, it provides an attractive target for designing inhibitors as potential antimicrobial drugs. The HTA in the present study is from *Leptospira interrogans* (*Li*HTA). *Leptospira* is an obligately aerobic, tightly coiled spirochaete, which is parasitic and can infect mammals to cause the water-borne zoonosis leptospirosis. *Leptospira* exhibits both transsulfuration and direct sulfhydrylation pathways for methionine biosynthesis [7–9]. In addition, HTA was identified as a potential therapeutic target since inactivation of HTA of *L. meyeri*, a nonpathogenic *Leptospira*, could result in methionine auxotrophy [9].

We were interested in determining structural basis for the substrate specificity and the underlying catalytic mechanism of the acetyl transfer reactions carried out by HTAs. The catalytic mechanism of HTA is different from that of the other acetyltransferases with known 3D structures.

Abbreviations: HTA, homoserine *O*-acetyltransferase; OAH, *O*-acetylhomoserine; CoA, coenzyme A; LiHTA, HTA from *Leptospira interrogans*; PMSF, phenylmethylsulfonyl fluoride; EDTA, ethylenediaminetetraacetic acid; IPTG, isopropyl-β-D-thiogalactopyranoside; DTT, dithiothreitol; DTNB, 5,5′-dithiobis(2-nitrobenzoic acid); TFE, 2,2,2-trifluoroethanol.

* Corresponding authors. Fax: +86 10 64888513.
E-mail addresses: hxu@moon.ibp.ac.cn (H. Xu), wgong@ibp.ac.cn (W. Gong).

[1] These authors contributed equally to this study.

0006-291X/$ - see front matter © 2007 Elsevier Inc. All rights reserved.
doi:10.1016/j.bbrc.2007.08.153

For instance, choline acetyltransferase and carnitine acetyltransferase recruit a single histidine in the active site [10,11]; serine acetyltransferase belongs to the left-handed β-helical family and uses the substrate serine itself as the nucleophile in the catalytic triad [12]; histone acetyltransferase has flanking domains implicated in histone binding and a central core domain harboring a putative catalytic base [13]. Whereas the HTAs belong to the expansive and diverse α/β hydrolase superfamily and contain the conserved catalytic triad in the active site.

This paper reports the X-ray structure of *Li*HTA determined at 2.2 Å, which is well defined by an overall conservation of the secondary structures of the α/β hydrolase superfamily. In addition, the catalytic histidine and serine of *Li*HTA are present in two conformations, which has not been observed in the previously reported structure of *Haemophilus influenzae* HTA (*Hi*HTA) [14]. Such double conformations may play some interesting roles in catalysis, which are discussed below.

Materials and methods

Expression and purification of recombinant LiHTA. *Li*HTA was amplified by PCR from genomic DNA and cloned in frame between the NdeI and XhoI restriction sites of pET22b (+) vector (Novagen). *Escherichia coli* BL21 (*DE3*) cultured in LB medium or B834 (*DE3*) cultured in M9 medium was used for expression of the recombinant native or selenomethionine substituted protein. Cells were grown at 37 °C until culture density reached OD_{600} 0.6–1.0. IPTG was added to give a final concentration of 0.8 mM and the culture was incubated for additional 4 h. Cells were harvested by centrifugation and resuspended in Buffer A (50 mM Tris–HCl, pH 8.0, 10 mM NaCl, 1 mM EDTA, and 1 mM DTT) supplemented with 1 mM PMSF. Lysis of the cells was carried out using sonication. After centrifugation, the clarified lysate was loaded on a DEAE–Sepharose Fast Flow column (Amersham) pre-equilibrated with Buffer A. Bound *Li*HTA was eluted using a linear gradient of NaCl (10–500 mM) over 10 column volumes. Fractions containing *Li*HTA were pooled, concentrated using 10 kDa cut-off centrifugal concentrators (Millipore) and applied to a Superdex 75 (Amersham) size exclusion column. All the purification operations were performed at 4 °C.

Biochemical assays. Acetyltransferase activity of *Li*HTA was measured according to Yamagata [15]. Protein concentration was determined by the method of Bradford [16]. Sedimentation velocity experiment was performed on a ProteomeLab XL-I analytical ultracentrifuge (Beckman Coulter) at 58,000 rpm and 20 °C, with the protein in 20 mM Tris–HCl, pH 8.0, and 150 mM NaCl.

Crystallization and data collection. Pure *Li*HTA (15 mg/ml in 50 mM Tris–HCl, pH 8.0, 150 mM NaCl) was used to set up crystallization trials at 277 K using the hanging-drop vapour-diffusion method. Each drop contained 1 μl protein solution and 1 μl reservoir solution. Initial screening was done using commercial sparse matrix kits—Crystal Screens I and II (Hampton Research) [17]. Freshly cleaved mica silanized by 3-aminopropyl triethoxysilane was used as the surface for setting up crystallization drops. Using above method diffraction resolution was improved as described by Tang et al. [18]. $0.2 \times \times 0.3 \times 0.4$ mm^3 size seleno-methionine substituted *Li*HTA crystals grew within a week with 10% PEG 20,000 and 0.1 M MES, pH 6.5. Native *Li*HTA crystal grew in a similar condition with additional 25% TFE while pH ranged from 6.5 to 7.5. Crystals were soaked briefly in mother liquor solutions containing increasing concentrations of glycerol (10%, 20%, and 30%) and finally flash-frozen at 100 K in a stream of nitrogen gas.

One 2.80 Å data set from a seleno-methionine substituted *Li*HTA crystal was collected at 100 K at the beamline 3W1A, Beijing Synchrotron Radiation Facility (BSRF), Institute of High Energy Physics, Chinese Academy of Sciences. One 2.20 Å data set from a native crystal was collected on a R-AXIS IV^{++} imaging-plate detector with Cu Kα X-rays (1.5418 Å) generated by a rotating-anode generator (Rigaku, Japan). All data sets were processed and scaled with HKL2000 [19].

Structure determination and refinement. SHELXD [20] was used to locate seven Se atoms. Diffraction phases to 2.80 Å resolution were calculated based on the seleno-methionine substituted *Li*HTA crystal data and improved with the program SOLVE [21]. The overall figure of merit (FOM) was 0.27. RESOLVE [22] improved the FOM to 0.69 and automatically located 60% of the residues. Program O [23] and CNS [24] were used to rebuild and manually connect the fragments and perform refinement for the initial model. The model was then refined against the higher quality diffraction data set to 2.20 Å using COOT [25] and REFMAC [26]. The statistics of structure refinement are summarized in Table 1. Stereochemical quality of the final model was checked by PROCHECK [27].

The atomic coordinates of *Li*HTA have been deposited into the Protein Data Bank (PDB Accession Code: 2PL5).

Results and discussion

Expression, purification, and enzymatic properties of LiHTA

*Li*HTA was overexpressed as a soluble protein in *E. coli* BL21 (DE3), and was purified by anion exchange and gel filtration chromatography. SDS–PAGE analysis of pure

Table 1
Crystallographic data collection and refinement statistics of *Li*HTA

Crystal	SeMet-*Li*HTA	*Li*HTA
Data collection statistics		
Wave length (Å)	0.9795	1.5418
Space group	$P4_32_12$	$P4_32_12$
Unit cell (Å)	$a = b = 61.4$, $c = 216.3$	$a = b = 61.1$, $c = 215.1$
Resolution range (Å)	50.00–2.80 (2.90–2.80)[a]	50.00–2.20 (2.28–2.20)
No. of unique reflections	10965	21812
Average redundancy	13.9 (12.9)	6.9 (7.0)
Completeness	99.6 (100.0)	99.6 (100.0)
R_{merge}[b] (%)	9.7 (38.2)	3.1 (19.0)
I/σ (I)	22.5 (4.5)	55.6 (11.7)
Refinement statistics		
R_{cryst}/R_{free}[c] (%)		21.6/25.8
R.m.s.d. bond length[d] (Å)		0.008
R.m.s.d. bond angle (°)		1.059
Number of protein residues		362
Number of water molecules		188
Average temperature factor (Å^2)		
Protein main-chain atoms		39.2
Protein side-chains atoms		39.5
Water molecules		45.6

$R_{free} = \Sigma_{SUB}||F_{obs}| - |F_{calc}||/\Sigma_T|F_{obs}|$, where T is a test data set of about 10% of the total reflections randomly chosen and set aside prior to refinement.

[a] Data for high-resolution bins are in parentheses.

[b] $R_{merge} = \Sigma|I_i - I_m|/\Sigma I_i$, where I_i is the intensity of the measured reflection and I_m is the mean intensity of all symmetry-related reflections.

[c] $R_{cryst} = \Sigma||F_{obs}| - |F_{calc}||/\Sigma|F_{obs}|$, where F_{obs} and F_{calc} are observed and calculated structure factors.

[d] R.m.s.d., Root-mean-square deviations.

*Li*HTA with or without DTT always showed a single band of protein approximately 40 kDa in size.

Enzyme activity was measured at four different concentrations of acetyl-CoA and five different concentrations of homoserine. The double reciprocal plots of initial velocity revealed parallel lines (data not shown), indicating a ping-pong mechanism, which is consistent with previous reports [28]. The Km values for acetyl-CoA and homoserine were 0.95 mM and 1.6 mM, respectively, determined by fitting the data to the equation for a ping-pong reaction.

Structure overview

The crystal structure solution of recombinant *Li*HTA was determined by the selenomethionyl single-wavelength anomalous diffraction (SAD) method [29]. The full length protein consists of 366 residues while the model accounts for residues 5–366. As shown in Fig. 1A, *Li*HTA is composed of 10 α-helices and 10 β-strands, which can be divided into two structurally distinct domains: a core α/β domain (residues 3–180 and 286–365) and a helical bundle "lid" domain (residues 181–285). The core α/β domain contains an eight-stranded mostly parallel β-sheet, with four α-helices (αB, αC, αD, αE) on one side and one (αF) on the other. Between β1 and β2 are two short additional antiparallel beta strands, β1′ and β1″. The lid domain is composed of five α-helices (αL1-5). The electron density of residues 251–268 (containing αL4) is weak, indicating some degree of flexibility. When no TFE was present in the crystallization condition, this fragment did not show any visible density above noise.

The structure of *Li*HTA shares the α/β hydrolase fold [30], consistent with the initial prediction based on the presence of the α/β hydrolase signature sequences. The topology of *Li*HTA is shown in Fig. 1B, with the core secondary structure elements named in accordance with the nomenclature used for the α/β hydrolase superfamily. Unsurprisingly, the overall structure of *Li*HTA is similar to that of the *H. influenzae* HTA (Fig. 2).

Dimerization of LiHTA

*Li*HTA forms a dimer through a crystal 2-fold axis and sedimentation velocity analysis of *Li*HTA resulted in a

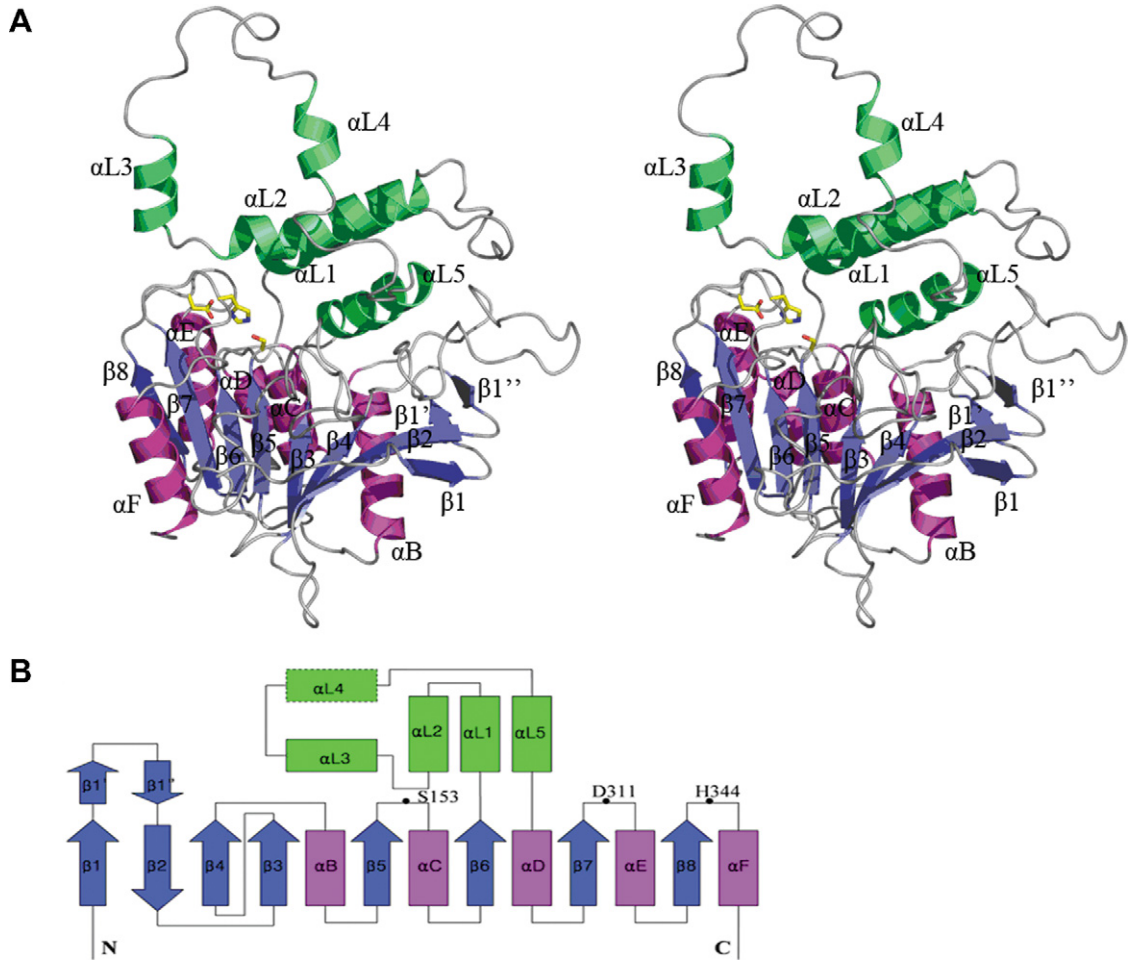

Fig. 1. Structure of *Li*HTA. (A) Stereoview of *Li*HTA in ribbon representation. The central β-sheet is colored cyan. The α-helices of the core α/β domain are in magenta, of the lid domain are in green. The classical conformations of 'catalytic triad'—S153, D311, and H344, were shown as sticks. (B) Schematic diagram of the topology of *Li*HTA with the three catalytic critical residues labeled. (For interpretation of the references to colour in this figure legend, the reader is referred to the web version of this article.)

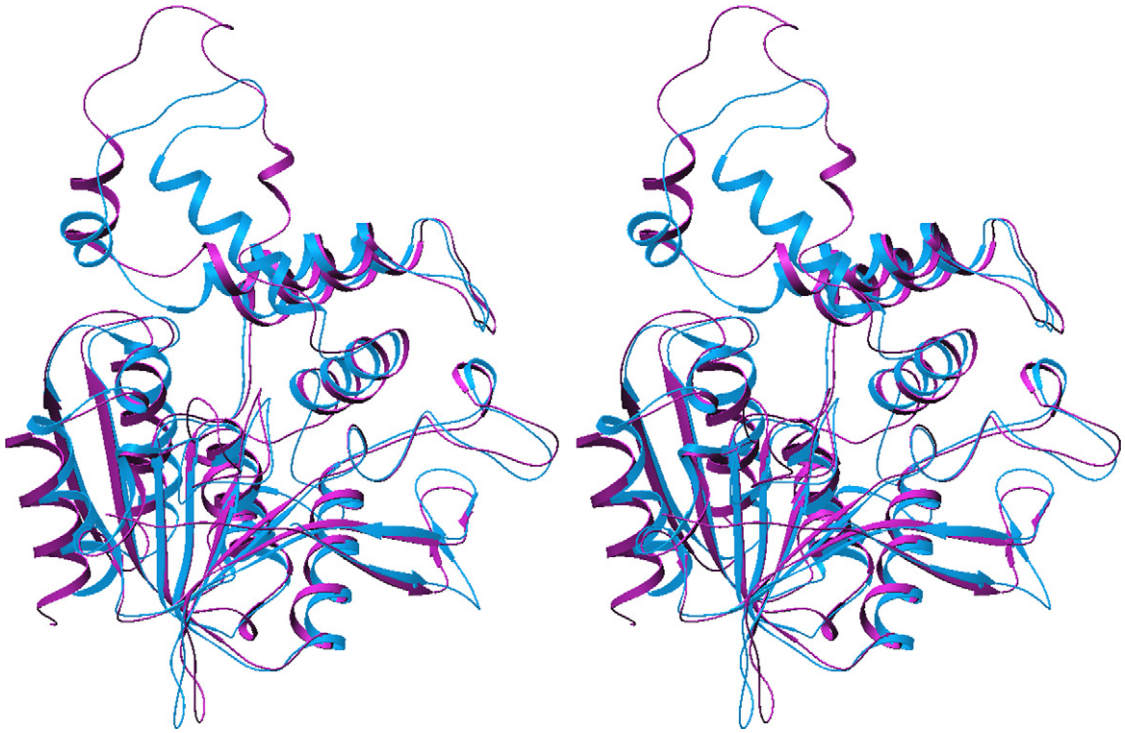

Fig. 2. Ribbon diagram showing the superimposition of *Li*HTA and *Hi*HTA. The structures were superposed using mainly the Cα atoms from the core α/β domain. *Li*HTA is shown in magenta and *Hi*HTA is shown in skyblue. (For interpretation of the references to colour in this figure legend, the reader is referred to the web version of this article.)

single peak with an apparent molecular weight of 77kD (data not shown), suggesting that *Li*HTA exists also as a dimer in solution. This is consistent with previous report that *H. influenzae* HTA is dimeric in both crystal and solution [14,28]. These two HTA dimers are formed in a similar way. Helix L1 and L2 from each subunit form an antiparallel four-helix bundle, in which the interface is predominantly hydrophobic. Helix L3 and L4 are also involved in the interaction of two subunits, stabilizing the dimeric structure [14]. Despite the above similarity, there is a prominent distinction between the two HTA dimers. In *Hi*HTA, the four-helix bundle is left-handed while that in *Li*HTA is right-handed.

Analysis of similar region in RsbQ (a stress–response regulator in *Bacillus subtilis*,PDB ID: 1WOM), a structural homolog of *Li*HTA (*Z*-score 22.3) found by the program Dali [31] with only 9% identity in sequence, shows that the residues corresponding to helix L4 form a 12-residue helical lid over the catalytic site [32]. Since the helix L4 is involved in the dimerization interface, it is therefore plausible that dimerization of *Li*HTA causes movement of this lid away from the active site, which is important for catalytic activity.

Double conformations of H344 and S153 in the active site

The critical conserved structural feature of α/β hydrolase is the catalytic triad, a constellation of three hydrogen bonded residues, a nucleophile, an acid and an absolutely conserved histidine. In the *Li*HTA structure, the catalytic triad is formed by S153 (nucleophile), D311 (acidic residue) and H344. These three residues are located on specific loops in *Li*HTA (Fig. 1A and B). D311 is located after strand β7 as in α/β hydrolase superfamily. S153 is located in the 'nucleophile elbow' between β5 and αC. The tightness of this strand-turn-helix motif induces S153 to adopt energetically unfavorable torsion angles in the disallowed region of the Ramachandran plot. H344 is located after the last β strand, and its backbone lies in generously allowed regions of the Ramachandran plot.

Interestingly, when we refined the structure of *Li*HTA, we found that H344 exists in two conformations (Fig. 3). These two conformations have similar occupancy, and the same double conformations were observed in all the structures from crystals grown under different pH range (pH 6.5–pH 7.5). In the first conformation (H344a), one hydrogen bond is formed between H344 ND1 and D311 OD1 and another between H344 NE2 and S153 OG (Fig. 4). In this "classical" triad conformation, H344 acts as a general base to activate S153 for nucleophilic attack at the thioester bond of acetyl-CoA. This catalytic triad was also observed as a single conformation in the recently reported structure of HTA from *H. influenzae* [14]. In the second conformation (H344b), H344 does not form any hydrogen bond with the other two members of the catalytic triad. Instead, H344 NE2 forms one hydrogen bond with T227 OG1, while H344 ND1 and D345 OD1 form a weak hydrogen bond (Fig. 4). The conformational change of the

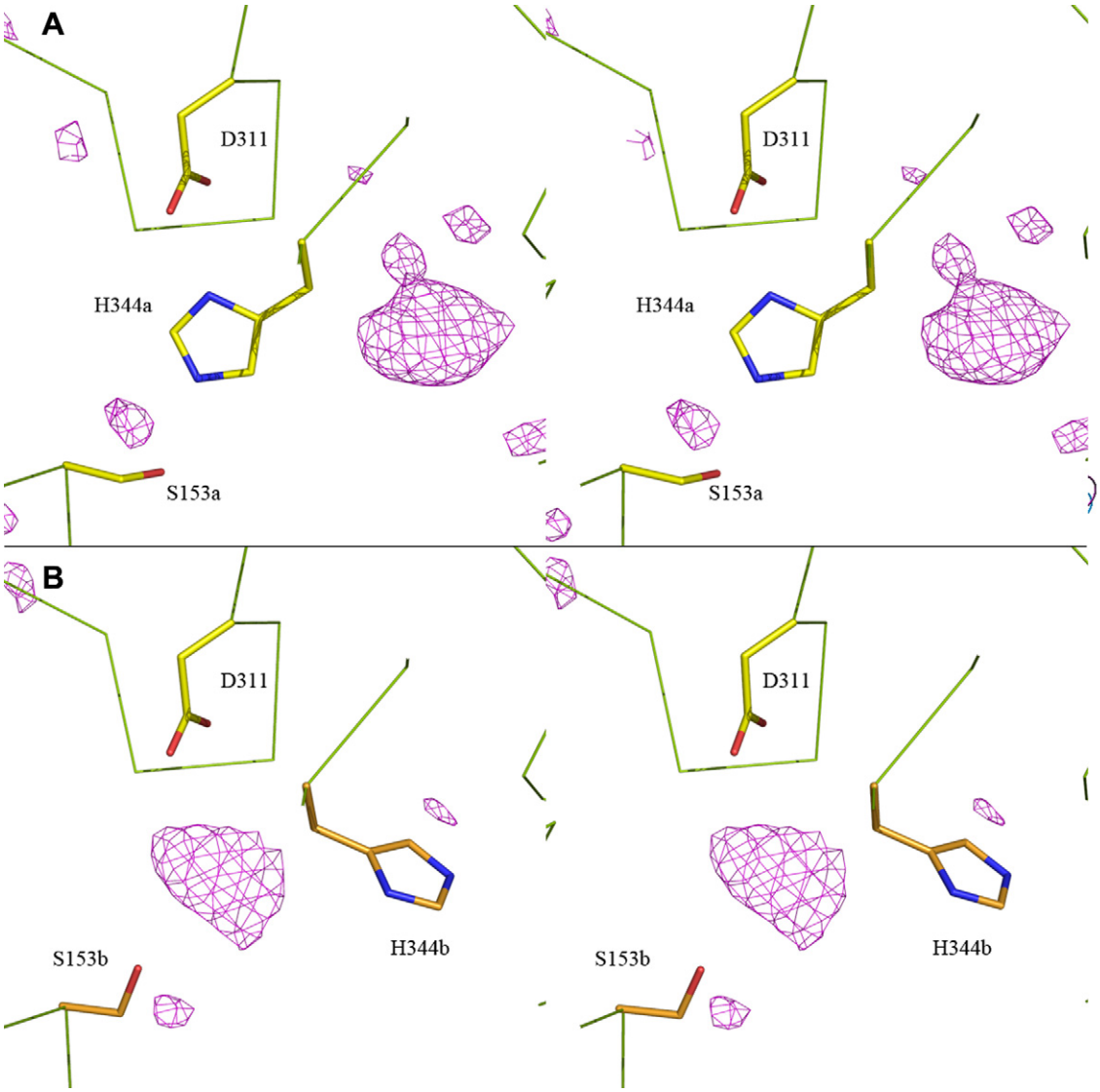

Fig. 3. Double conformations of H344 and S153. (A) H344 and S153 in the classical conformation; (B) H344 and S153 in the second conformation. F_o–F_c omit map contoured at 3.0σ is in purple. (For interpretation of the references to colour in this figure legend, the reader is referred to the web version of this article.)

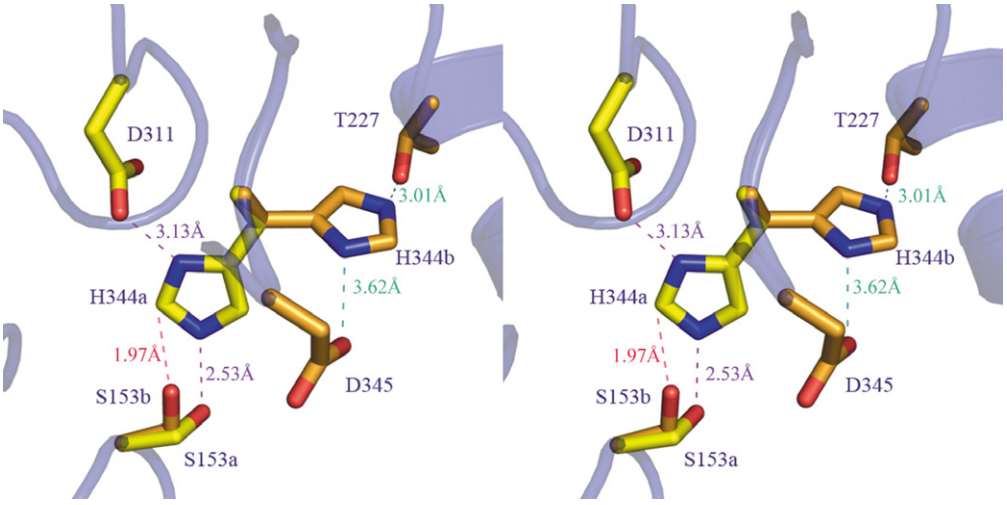

Fig. 4. Stereoview of the alternative conformations of catalytic activity related residues. In the first conformation, H344a forms hydrogen bonds with S153a and D311. While in the second conformation, H344b forms hydrogen bonds with D345b and T227.

histidine during catalysis was previously reported for chymotrypsin, where a 20° shift of dihedral angle $\chi 1$ of the catalytic histidine was experimentally observed and agreed with *ab initio* calculations [33]. This conformational change in chymotrypsin is energetically more favorable for turning the abstracted proton towards the nitrogen of the scissile bond in substrate. However in the case of *Li*HTA, the conformational change of H344 results in a much larger, almost 180°, rotation of the $\chi 1$ rotamers. This large movement is more likely to make room for the homoserine to enter and bind at the active site, followed by a nucleophilic attack on the ester linkage of the acetyl-HTA intermediate.

The catalytic residue S153 also exists in two conformations. Compared with the classical triad, where S153 (S153a) OG forms a hydrogen bond with H344a NE2, S153 OG in the second conformation (S153b) is only 1.97 Å away from H344a CE1 (Fig. 4). This distance precludes the coexistence of S153b and H344a. S153b should only occur when the imidazole ring of H344 sways to second conformation. Therefore the double conformations of S153 and H344 agreed with each other well. Although some explanations have been proposed above, the biological significance of such conformational changes within the *Li*HTA catalytic site requires further investigation.

Acknowledgments

We acknowledge Prof. Peng Liu and Yuhui Dong in Institute of High Energy Physics and Yi Han in Institute of Biophysics for diffraction data collection. We also thank Dr Neil Shaw for critical reading and correction. This work is supported by National Foundation of Talent Youth (Grant No. 30225015), the 973 program (No. 2004CB520801), National Natural Science Foundation of China (Grant No.10490913 and No. 30500100) and Chinese Academy of Sciences (KSCX2-SW-224).

References

[1] J. Giovanelli, Sulfur amino acids of plants, Methods Enzymol. 143 (1987) 419–426.
[2] I. Saint-Girons, C. Parsot, M.M. Zakin, O. Barzu, G.N. Cohen, Methionine biosynthesis in Enterobacteriaceae: biochemical, regulatory, and evolutionary aspects, CRC Crit. Rev. Biochem. 23 (Suppl. 1) (1988) S1–S42.
[3] G.A. Marzluf, Genetics and molecular genetics of sulfur assimilation in the fungi, Adv. Genet. 31 (1994) 187–206.
[4] D. Thomas, Y. Surdin-Kerjan, Metabolism of sulfur amino acids in *Saccharomyces cerevisiae*, Microbiol. Mol. Biol. Rev. 61 (1997) 503–532.
[5] H. Ozaki, I. Shiio, Methionine biosynthesis in Brevibacterium flavum: properties and essential role of *O*-acetylhomoserine sulfhydrylase, J. Biochem. (Tokyo) 91 (1982) 1163–1171.
[6] T. Langin, G. Faugeron, C. Goyon, A. Nicolas, J.L. Rossignol, The MET2 gene of *Saccharomyces cerevisiae*: molecular cloning and nucleotide sequence, Gene 49 (1986) 283–293.
[7] J. Belfaiza, A. Martel, D. Margarita, I. Saint Girons, Direct sulfhydrylation for methionine biosynthesis in *Leptospira meyeri*, J. Bacteriol. 180 (1998) 250–255.
[8] S.X. Ren, G. Fu, X.G. Jiang, R. Zeng, Y.G. Miao, H. Xu, Y.X. Zhang, H. Xiong, G. Lu, L.F. Lu, H.Q. Jiang, J. Jia, Y.F. Tu, J.X. Jiang, W.Y. Gu, Y.Q. Zhang, Z. Cai, H.H. Sheng, H.F. Yin, Y. Zhang, G.F. Zhu, M. Wan, H.L. Huang, Z. Qian, S.Y. Wang, W. Ma, Z.J. Yao, Y. Shen, B.Q. Qiang, Q.C. Xia, X.K. Guo, A. Danchin, I. Saint Girons, R.L. Somerville, Y.M. Wen, M.H. Shi, Z. Chen, J.G. Xu, G.P. Zhao, Unique physiological and pathogenic features of *Leptospira interrogans* revealed by whole-genome sequencing, Nature 422 (2003) 888–893.
[9] M. Picardeau, H. Bauby, I. Saint Girons, Genetic evidence for the existence of two pathways for the biosynthesis of methionine in the *Leptospira* spp., FEMS Microbiol. Lett. 225 (2003) 257–262.
[10] G. Jogl, L. Tong, Crystal structure of carnitine acetyltransferase and implications for the catalytic mechanism and fatty acid transport, Cell 112 (2003) 113–122.
[11] Y. Cai, C.N. Cronin, A.G. Engel, K. Ohno, L.B. Hersh, D.W. Rodgers, Choline acetyltransferase structure reveals distribution of mutations that cause motor disorders, EMBO J. 23 (2004) 2047–2058.
[12] V.E. Pye, A.P. Tingey, R.L. Robson, P.C. Moody, The structure and mechanism of serine acetyltransferase from *Escherichia coli*, J. Biol. Chem. 279 (2004) 40729–40736.
[13] R. Marmorstein, Structure of histone acetyltransferases, J. Mol. Biol. 311 (2001) 433–444.
[14] I.A. Mirza, I. Nazi, M. Korczynska, G.D. Wright, A.M. Berghuis, Crystal structure of homoserine transacetylase from *Haemophilus influenzae* reveals a new family of alpha/beta-hydrolases, Biochemistry 44 (2005) 15768–15773.
[15] S. Yamagata, Partial purification and some properties of homoserine *O*-acetyltransferase of a methionine auxotroph of *Saccharomyces cerevisiae*, J. Bacteriol. 169 (1987) 3458–3463.
[16] M.M. Bradford, A rapid and sensitive method for the quantitation of microgram quantities of protein utilizing the principle of protein-dye binding, Anal. Biochem. 72 (1976) 248–254.
[17] J.K. Jancarik, S.-H. J. Kim, Appl. Cryst. 24 (1991) 409–411.
[18] L. Tang, Y.B. Huang, D.Q. Liu, J.L. Li, K. Mao, L. Liu, Z.J. Cheng, W.M. Gong, J. Hu, J.H. He, Effects of the silanized mica surface on protein crystallization, Acta Crystallogr. D Biol. Crystallogr. 61 (2005) 53–59.
[19] W. Minor, Z. Otwinowski, Processing of X-ray diffraction data collected in oscillation mode, Methods Enzymol. 276 (1997) 307–326.
[20] T.R. Schneider, G.M. Sheldrick, Substructure solution with SHELXD, Acta Crystallogr. D Biol. Crystallogr. 58 (2002) 1772–1779.
[21] T.C. Terwilliger, J. Berendzen, Automated MAD and MIR structure solution, Acta Crystallogr. D Biol. Crystallogr. 55 (Pt 4) (1999) 849–861.
[22] T.C. Terwilliger, Maximum-likelihood density modification, Acta Crystallogr. D Biol. Crystallogr. 56 (Pt 8) (2000) 965–972.
[23] T.A. Jones, J.Y. Zou, S.W. Cowan, Kjeldgaard, Improved methods for building protein models in electron density maps and the location of errors in these models, Acta Crystallogr. A 47 (Pt 2) (1991) 110–119.
[24] A.T. Brunger, P.D. Adams, G.M. Clore, W.L. DeLano, P. Gros, R.W. Grosse-Kunstleve, J.S. Jiang, J. Kuszewski, M. Nilges, N.S. Pannu, R.J. Read, L.M. Rice, T. Simonson, G.L. Warren, Crystallography & NMR system: a new software suite for macromolecular structure determination, Acta Crystallogr. D Biol. Crystallogr. 54 (Pt 5) (1998) 905–921.
[25] P. Emsley, K. Cowtan, Coot: model-building tools for molecular graphics, Acta Crystallogr. D Biol. Crystallogr. 60 (2004) 2126–2132.
[26] M.D. Winn, G.N. Murshudov, M.Z. Papiz, Macromolecular TLS refinement in REFMAC at moderate resolutions, Methods Enzymol. 374 (2003) 300–321.
[27] M.W. McArthur, R.A. Laskowski, D.S. Moss, J.M. Thornton, PROCHECK: a program to check the stereochemical quality of protein structures, J. Appl. Cryst. 26 (1993) 283–291.
[28] T.L. Born, M. Franklin, J.S. Blanchard, Enzyme-catalyzed acylation of homoserine: mechanistic characterization of the *Haemophilus*

influenzae met2-encoded homoserine transacetylase, Biochemistry 39 (2000) 8556–8564.

[29] Z. Dauter, M. Dauter, E. Dodson, Jolly SAD, Acta Crystallogr. D Biol. Crystallogr. 58 (2002) 494–506.

[30] D.L. Ollis, E. Cheah, M. Cygler, B. Dijkstra, F. Frolow, S.M. Franken, M. Harel, S.J. Remington, I. Silman, J. Schrag, et al., The alpha/beta hydrolase fold, Protein Eng. 5 (1992) 197–211.

[31] L. Holm, C. Sander, Protein structure comparison by alignment of distance matrices, J. Mol. Biol. 233 (1993) 123–138.

[32] T. Kaneko, N. Tanaka, T. Kumasaka, Crystal structures of RsbQ, a stress–response regulator in *Bacillus subtilis*, Protein Sci. 14 (2005) 558–565.

[33] P. Hudaky, A. Perczel, Conformation dependence of pK(a): ab initio and DFT investigation of histidine, J. Phys. Chem. A 108 (2004) 6195–6205.